A correlation to evaluate cyclic resistance from CPT applied to a case history

Daniela Giretti & Vincenzo Fioravante

Bulletin of Earthquake Engineering
Official Publication of the European Association for Earthquake Engineering

ISSN 1570-761X

Bull Earthquake Eng
DOI 10.1007/s10518-016-0057-7

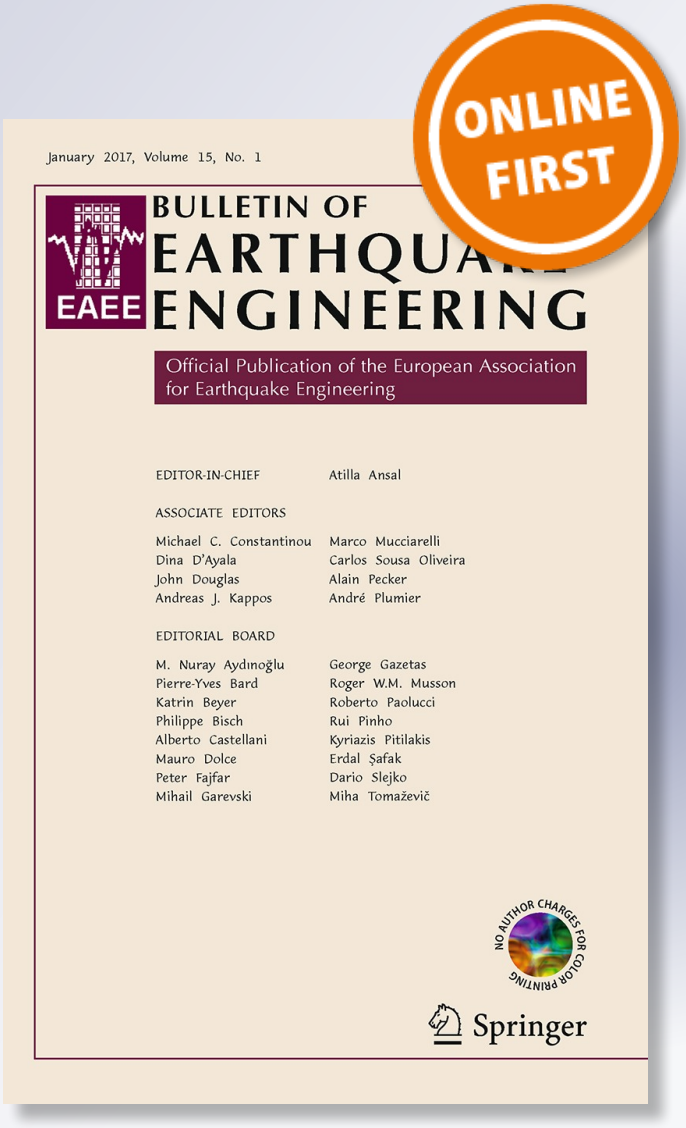

Springer

Bull Earthquake Eng
DOI 10.1007/s10518-016-0057-7

ORIGINAL RESEARCH PAPER

A correlation to evaluate cyclic resistance from CPT applied to a case history

Daniela Giretti[2,3] · **Vincenzo Fioravante**[1,3]

Received: 11 July 2016 / Accepted: 18 November 2016

Abstract A methodology to evaluate the undrained cyclic resistance of sandy deposits from cone penetration tests through the state parameter is applied to the case history of the village of San Carlo (Italy), where widespread liquefaction phenomena occurred during the 2012 Emilia earthquake. The mechanical behaviour of the sand retrieved in the area of San Carlo was characterised within the framework of critical state soil mechanics via a series of monotonic and cyclic triaxial tests carried out on both undisturbed and reconstituted samples. Centrifuge cone penetration tests were also performed on reconstituted models of the same material. The results of centrifuge and undrained cyclic triaxial tests were interpreted through the state parameter to calibrate a direct correlation between the cone resistance, q_c and the undrained cyclic resistance ratio (CRR). CRR profiles were deduced from the CPTs performed at sites in San Carlo where liquefaction took place using the correlation calibrated herein and a liquefaction assessment was carried out. The results of the proposed method was compared to a well-known simplified approach.

Keywords Liquefaction · Cyclic resistance · Sand · State parameter · Cone penetration tests · Centrifuge tests · Cyclic triaxial tests · Emilia earthquake

✉ Vincenzo Fioravante
vincenzo.fioravante@unife.it

Daniela Giretti
daniela.giretti@unibg.it

[1] University of Ferrara, Via Saragat 1, Ferrara, Italy

[2] University of Bergamo, Bergamo, Italy

[3] ISMGEO, Seriate, Bergamo, Italy

Published online: 19 December 2016

1 Introduction

In the months of May and June 2012, the Italian region between Emilia Romagna, Lombardia and Veneto (in the central-eastern part of the Po Plain) was shaken by a series of earthquakes (the Emilia seismic sequence, which lasted over two months and was characterised by more than 2000 shocks), of which the two main events are the May 20 and May 29 earthquakes, characterised by moment magnitude and hypocentre depth of $M_w = 5.8$ and $d_h = 9.5$ km, $M_w = 5.6$ and $d_h = 8.1$ km, respectively (iside.rm.ingv.it). As shown in Fig. 1, the epicentre of the May 20 shock was located nearly 30 km WNW of the city of Ferrara, in the municipality of Finale Emilia. The epicentre of the May 29 earthquake occurred in the area between Mirandola, Medolla e San Felice sul Panaro.

Despite the relative low magnitude of these earthquakes, they caused 27 deaths and widespread damage to residential, industrial and historical buildings, mainly due to the fact that the epicentral areas were declared seismic in 2003 and, consequently, only recent buildings were designed according to seismic criteria.

The two main shocks of the seismic sequence caused widespread liquefaction in various areas of the Emilia Romagna Region, whose surficial effects were craters, sand boils, surface ruptures and fissures and lateral spreading. Particularly, the May 20 shake produced significant liquefaction effects in the localities of San Carlo and Mirabello, which are located about 15 km SE of the epicentre (in the Ferrara Province, see Fig. 1). The consequences of soil liquefaction were tilt of buildings and lateral movements of foundations. However, these liquefaction phenomena aroused much interest because for the first time in recent years in Italy they occurred in residential areas and because many of the towns of the Po Valley (including Renaissance cities of high artistic value) are located in areas characterized by geological and geotechnical subsoil conditions similar to those of San Carlo and Mirabello.

After the May 20 and 29 earthquakes, many in situ geophysical and geotechnical tests and laboratory tests were carried out in order to evaluate the current condition of the subsoil of the sites where liquefaction occurred. The in situ tests included continuous

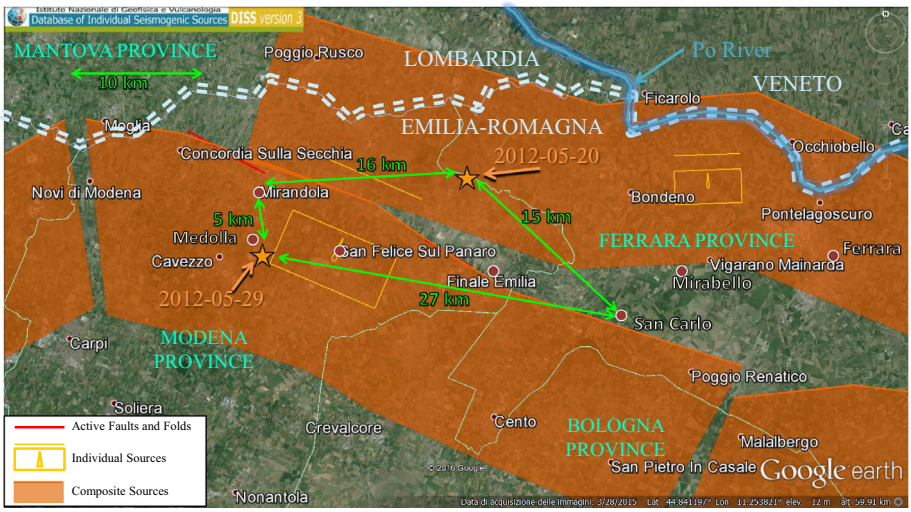

Fig. 1 Areas struck by the Emilia seismic sequence

borings and thin-walled tube sampling, cone penetration tests (CPT) and seismic cone penetration tests (SCPT), down-hole tests (DH) and ambient noise measurements. The laboratory tests on the retrieved samples included grain size analyses, index properties evaluation, monotonic undrained triaxial tests and resonant column tests.

A considerable part of the geotechnical tests were focused on the analysis of the mechanical behaviour of the sand affected by liquefaction at the site of San Carlo (where the larger amount of liquefaction phenomena were registered), hereafter referred to as SCS (San Carlo Sand). In addition to the standard laboratory tests mentioned above, cyclic undrained triaxial tests and centrifuge cone penetration tests were also carried out on SCS, with the main aim of calibrating a direct correlation between its cone and cyclic resistance. The experimentation followed the lines of a previous study carried out on two standard sands, Ticino and Toyoura, reported by Fioravante and Giretti (2016). The correlation was established referring to the state parameter ψ (i.e. the distance along the void ratio axis of a given state from the critical state line, Been and Jefferies 1985) as indicator of the state (stress level and density) and resistance of the soil.

This paper presents the mechanical characterisation of SCS, the results of cyclic triaxial and centrifuge tests and the calibration of the ψ-based correlation for estimating CRR from the cone resistance. The correlation was applied to the CPTs carried out at the site of San Carlo and the computed CRR profiles were compared to those computed with the Idriss and Boulanger (2008) method.

2 Local geology and liquefaction effects

The areas struck by the Emilia seismic sequence are located in the central-eastern part of the Po Plain, which is the foreland basin of the S-verging Central-Southern Alps and of the N-NE-verging Northern Apennines fold-and-thrust belts. The basin is filled by Plio-Quaternary marine and continental sediments, whose thickness extends from several thousand meters to less than one hundred of meters in correspondence of the crest of buried anticlines (Bigi et al. 1992).

Below the epicentral areas, the outermost NE-verging fronts of the Northern Apennines, known as Ferrara-Romagna folds, are buried and there are small surface signs of their tectonic activity (Toscani et al. 2009). These folds, which originated the 2012 seismic sequence, are constituted by two main arcs. The inner arc (the Mirandola Arc) has its crest between Novi di Modena, Mirandola and Poggio Renatico. The outer arc (the Ferrara Arc) has its peak between Bondeno, Occhiobello and Ferrara (see Fig. 1).

The Quaternary continental sediments in the epicentral areas are characterised by sequences of fine grained (permeability barriers) and coarse grained (aquifers) alluvial deposits, alternatively generated during marine transgressive and regressive phases and deposited by the Po river and its tributary rivers. Two principal stratigraphic units can be recognised, associated to two main alluvial cycles of the Po Plain: the Lower Emilia Romagna Synthem (650–450 kyr) and the Upper Emilia Romagna Synthem (450 kyr–present), (RER–EniAgip 1998). The base of the Lower Emilia-Romagna Synthem corresponds to the top of the marine succession.

The uppermost Quaternary succession (20–30 m below the ground surface) is ascribed to the Holocene and mainly consists of fine grained deposits with inclusions of ribbon-like fluvial-channel sandy deposits, of post-Last Glacial Maximum age (18 kyr-Present). In the

epicentral areas, these deposits can be attributed to the depositional activity of the Po river and its Apennine tributaries.

As to the localities of San Carlo and Mirabello, which were affected by extensive liquefaction during the May 20 earthquake, their territories have a common recent geological history, characterized by the sedimentary dynamic of the Reno river. The geological arrangements of the subsoil was deduced from a large number of in situ tests, including cone penetration tests and seismic cone penetration tests, continuous core and destructive core drillings and down hole tests, as represented in the map of the locality of San Carlo (Fig. 2a). As shown in Fig. 2b, where a stratigraphic section of San Carlo is reported (Calabrese et al. 2012), the subsoil is characterized within a depth of 30 m by three depositional units corresponding to three distinct sedimentary phases.

The two deeper units have an almost horizontal stratification: the lower one dates to the upper Pleistocene (last glaciation, Würm regression) and mainly consists of clean sands and silty sands typical of alluvial plain; the intermediate unit (Holocene) consists of clay, organic clay and peats, typical of swamp deposits. The upper unit consists of sandy silt,

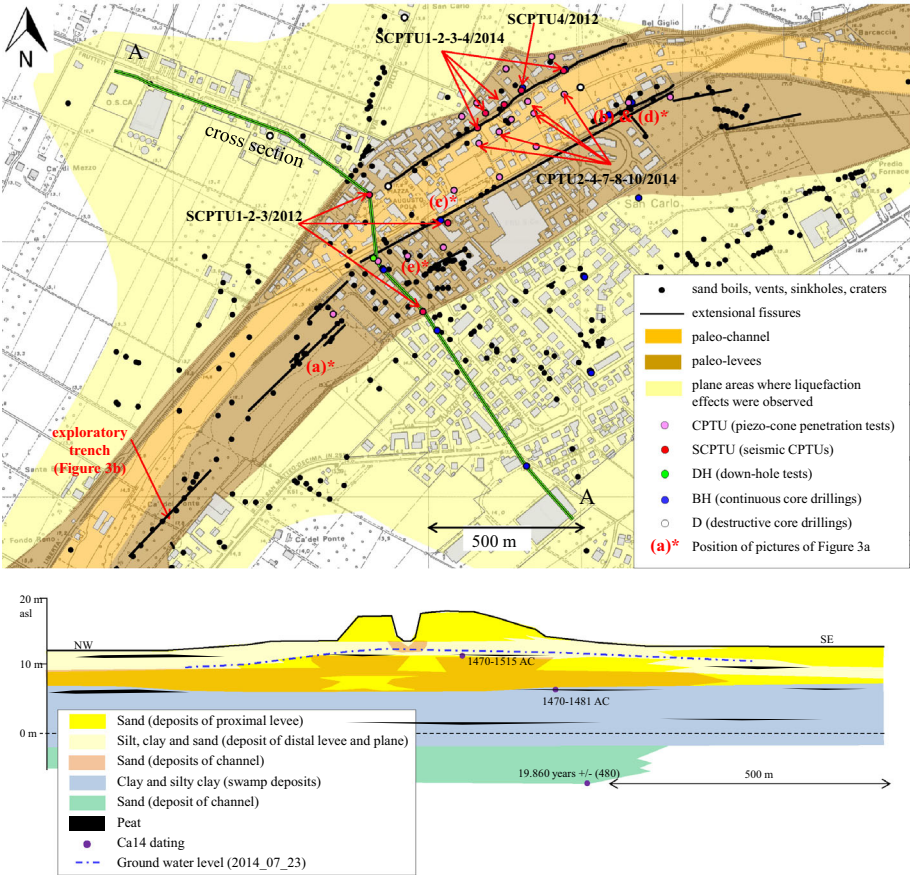

Fig. 2 Geological arrangement of the subsoil of San Carlo: **a** plane view and **b** A-A cross-section (from Calabrese et al. 2012)

silty sand and sand (deposits of channel and levee, whose plane view is shown in Fig. 2a, Calabrese et al. 2012) and was formed by the fluvial activity of the Reno river in the years between 1450 (to which date four samples of peat retrieved at the base of the sandy deposits, as deduced from carbon-14 dating) and 1770, after which the river was diverted. The sedimentation rate was very high, about 0.1–0.3 m per year, mainly due to the cold period which characterized the northern hemisphere in the years from about 1350 to about 1850 (known as Little Ice Age). Today, the abandoned channel and levees (paleochannel and paleolevees) of the Reno river form an area morphologically higher than the surroundings (generally flat) and house the historic cores of San Carlo and Mirabello. The levees are characterised by gentle slope of few degrees.

The sandy deposits of the upper unit house a phreatic aquifer, whose free surface is about 4 m deep from the top of the banks (1 m from the channel level) and has an annual variability lower than 1 m.

The soils affected by liquefaction during the 20 May earthquake are the sandy layers of the upper unit located below the ground water table, as demonstrated by a 6 m deep trench within which it was possible to observe the soil profile and the paths followed by the rising sand (see Fig. 3b).

Liquefied sand break out and submerged large areas of San Carlo and Mirabello. The surface effects observed after the main shock were mainly concentrated along sloping areas crossed by the river paleobanks and paleochannel and consisted in surface ruptures, extensional fissures, sand boils, vents, sinkholes and craters (see the map in Fig. 2a, where their locations are reported). The top of the banks slipped towards the channel. Roads and open spaces were flooded by the erupted sand and water. The thickness of the ejected soil was often of the order of tens of centimetres. Locally, gas and water pipelines were damaged and roads were cracked. As to the buildings, liquefaction caused tilting and overturning of foundations, which however still supported well the structures (Fioravante et al. 2013). Figure 3a reports some pictures taken immediately after the 20 May earthquake. Figure 3b presents pictures taken from a 6 m deep trench excavated across an extensional fissure to observe the local stratigraphy.

3 Ground motion characteristics

The area affected by the Emilia seismic sequence is characterised by moderate seismicity. The most relevant historic earthquake dates back to 1570, November 17 (macro-seismic intensity I_{MCS} = VII–VIII) and struck the city of Ferrara and its surroundings. The main shock was followed by a long sequence of aftershocks, which lasted up to 1572. Liquefaction evidences were observed (Galli and Melloni 1993).

The 2012 seismic sequence was characterised by two main shocks (May 20 and 29) of moment magnitude $M_w = 5.8$ and $M_w = 5.6$, respectively, both followed by dozens of aftershock characterised by $M_w > 3$, of which six had $M_w \geq 5$ (see Table 1, iside.rm.ingv.it). The epicentre of the May 20 shock was located nearly 30 km WNW of the town of Ferrara, in the municipality of Finale Emilia; the epicentre of the May 29 earthquake occurred in the area between Mirandola, Medolla e San Felice sul Panaro. Starting from the first main shock, the epicentres progressively shifted westwards, covering an area about 50 km in the E–W direction and 15 km in the N–S direction and revealing the activation of a complex thrust front system composed by at least two main distinct invers faults, belonging to the Ferrara and Mirandola arcs (Lavecchia et al. 2012). Figure 4

Fig. 3 **a** Liquefaction effects and **b** 6 m deep exploratory trench

represents the spatial distribution of the shocks characterised by $M_w > 3$ registered between May 20 and June 30 (date within which about 90% of the total number of earthquakes of the sequence had occurred).

The RAN (Italian Strong Motion Network) permanent stations closest to the May 20 shock epicentre was the Mirandola station (MRN, soil class C), located at a distance of

Table 1 Earthquakes of M > 5 (*Source*: iside.rm.ingv.it)

Time (UTC)		Depth (km)	Magnitude	Latitude	Longitude
2012/05/20	02:03:50.170	9.5	5.8 (M_w)	44.896	11.264
2012/05/20	02:07:28.950	6.1	5.0 (M_L)	44.874	11.27
2012/05/20	03:02:47.090	9.1	5.0 (M_L)	44.86	11.152
2012/05/29	07:00:02.880	8.1	5.6 (M_w)	44.842	11.066
2012/05/29	08:25:51.480	7.9	5.0 (M_L)	44.865	10.948
2012/05/29	10:55:56.550	4.4	5.3 (M_w)	44.865	10.98
2012/05/29	11:00:01.680	8.7	5.0 (M_L)	44.856	10.941
2012/05/29	11:00:22.990	7.2	5.1 (M_L)	44.866	10.976

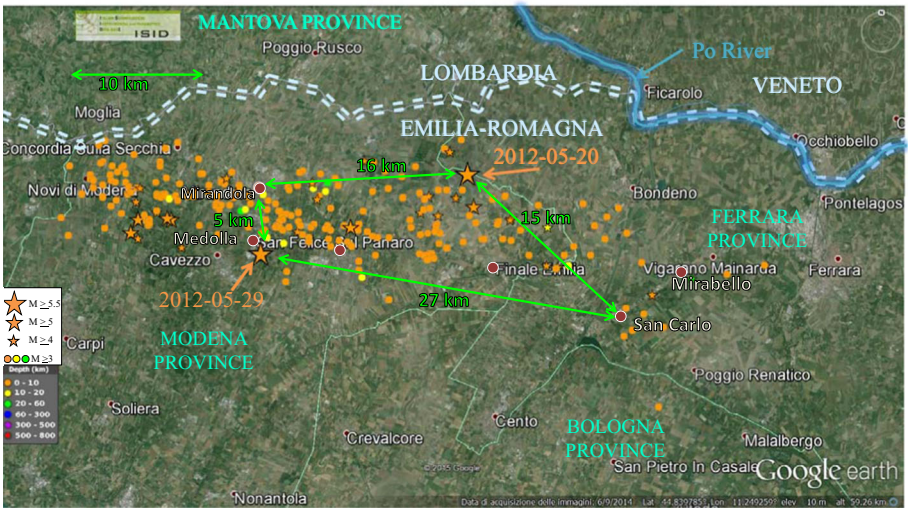

Fig. 4 Seismic sequence epicenters

Table 2 Main seismic parameters of the May 20 and 29 earthquakes, registered at the MRN station (Mirandola is the station closest to both the epicentres of May 20 and 29 earthquakes, data from DPC-RAN, http://ran.protezionecivile.it)

	2012/05/20					2012/05/29				
	PGA (g)	PGV (cm/s)	PGD (cm)	Housner (cm)	Arias (cm/s)	PGA (g)	PGV (cm/s)	PGD (cm)	Housner (cm)	Arias (cm/s)
NS	0.264	47.9	14	170	78	0.295	57.1	17	180	120
EW	0.261	29.5	9.2	110	64	0.224	28.6	8.7	100	72
UP	0.309	5.9	2.3	24	45	0.889	27.8	10	53	300

PGA peak ground acceleration, *PGV* peak ground velocity, *PGD* peak ground displacement, *Housner* Housner spectral intensity, *Arias* Arias intensity

about 16 km to the West of the epicentre. After the first main shock, 17 additional temporary stations were installed in the epicentral area. The closer station to the May 29 seismic event epicentre, was again the MRN, located at a distance of about 5 km to the Nord of the epicentre. The main parameters of the two shocks recorded by the MRN station are reported in Table 2. For the May 20 event, a horizontal peak acceleration of about 0.26 g was recorded. Both NS and EW components had similar peak accelerations values; the vertical PGA was slightly higher, equal to 0.31 g. In the case of the May 29 quake, the horizontal PGA in the EW and NS components were 0.224 g and 0.295 g, respectively. The peak ground vertical acceleration was as high as 0.889 g (DPC-RAN, http://ran.protezionecivile.it).

On the basis of the recorded accelerations of the May 20 and 29 shocks, the National Institute of Geophysics and Volcanology (INGV, http://shakemap.rm.ingv.it/shake/index.html) produced PGA shake maps. At San Carlo (where no recording stations were installed before the shocks), a horizontal PGA of 0.16 g was estimated for the 20 May earthquake, during which liquefaction occurred. During the May 29 shock, when liquefaction phenomena were not recorded in the area of interest, a temporary station installed 3 km from San Carlo, measured a horizontal PGA of 0.08 g.

4 Geotechnical characteristics of the site of San Carlo

The village of San Carlo was one of the most affected by liquefaction effects during the May 20 earthquake. For this reason many in situ investigations were concentrated in its territory; their type and distribution are represented in Fig. 2a and summarised in Table 3. Figure 5 reports the results of the seismic piezocone tests (SCPTUs), in terms of cone resistance q_c (Fig. 5a) and shear wave velocity V_S (Fig. 5b) plotted versus the altitude above the sea level. The SCPTUs were all performed from the top of the paleobanks. Figure 6 shows the results of five cone penetration tests (CPTUs) carried out from the centre of the paleochannel. In Fig. 7 are represented the results of the index tests carried out on the undisturbed samples (which were mainly retrieved from boreholes performed from the top of the banks), in terms of grading, mean diameter (D_{50}), fines content (FC), natural water content (w_n), liquid limit (LL), plastic limit (LP) and plasticity index (IP).

Table 3 Geotechnical in situ tests carried out in the village of San Carlo

Type of test	No.	Maximum depth (m)	No. of undisturbed samples	No. of dissipation tests
BH	6	8–10	7	
	7	11–13	9	
	4	30	17	
	1	40	3	
D	4		–	
CPTU	10	20		–
	10	30		10
SCPTU	8	30		2
DH	1	40		

BH continuous core drillings, *D* destructive core drillings, *CPTU* piezocone penetration test, *SCPTU* seismic piezocone penetration test, *DH* down-hole test

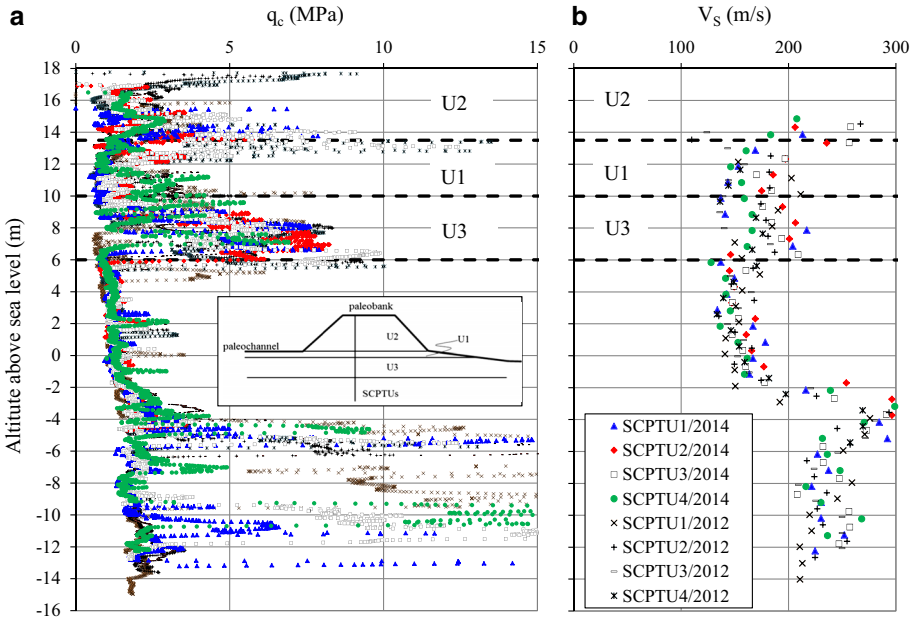

Fig. 5 Results of 8 SCPTUs carried out from the top of the paleobanks: **a** cone resistance q_c and **b** shear wave velocity V_S versus the altitude above the sea level

Overall, the tests show a certain repeatability of the soil characteristics (see also Fig. 2b). The soils present from 18 to 5–6 m above the sea level belong to the deposits of the Reno river. Three distinct lithological sub-units can be distinguished. The unit forming the paleobanks (U2) which is located from about 18 m to 13–14 m above the sea level, is characterised by sandy silt and silty sand, an average FC (diameter <0.075 mm) of about 48% and an average clay fraction (CF) of about 9%. Below the banks there is an almost horizontal layer, from 2 to 4 m thick, of sandy and clayey silt (U1, average FC $\approx$ 76%, average CF $\approx$ 15%), followed by a layer of sand from 2 to 4 m thick (up to 6 m in correspondence of the centre of channel), with a FC lower than 20–25%. This sandy layer (U3) represents the channel deposits of the Reno river, which were affected by liquefaction during the 20 May earthquake.

As evidenced in Figs. 5 and 6, U3 is characterised by an average cone resistance $q_c \approx 4$ MPa, which increases with depth, and average shear wave velocity $V_S \approx 180$ m/s. The fines present in the Reno river deposits are generally characterised by low plasticity. The grain size curves measured on the undisturbed samples retrieved in the 3 sub-units U1, U2 and U3 are shown in Fig. 8. Except for four specimens, all the grain size analyses on U3 samples evidenced almost uniform sand, with a fine content lower than 20%.

Below U3, a continuous layer 8 to 10 m thick of plastic fine grained soils follows, composed of silty clay from 6 to 0 m above the sea level and clayey silt from 0 to −4 m above the sea level. Finally, a sequence of sandy and fine grained layers is present up to the maximum investigated depth of 40 m below ground surface (Table 3).

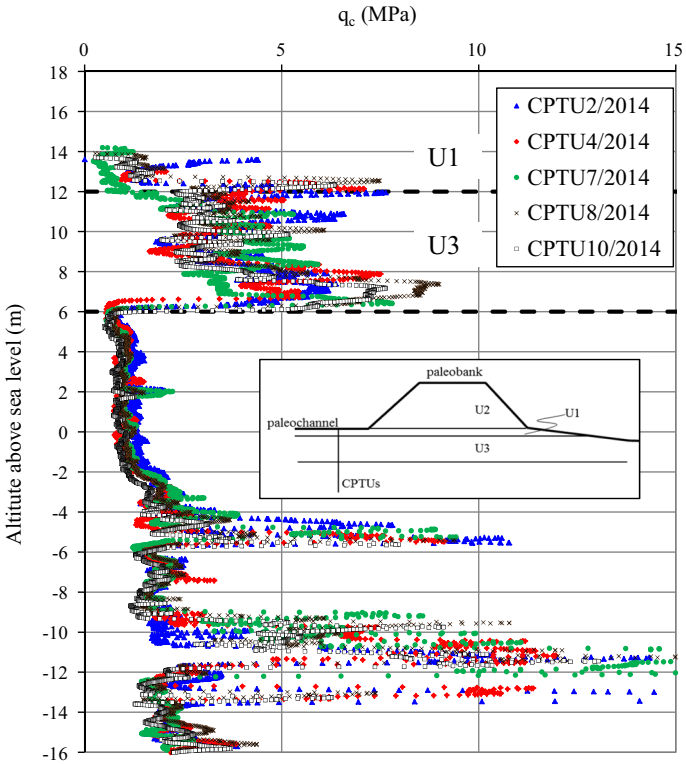

Fig. 6 Results of the 5 CPTUs carried out from the center of the paleochannel: cone resistance q_c versus the altitude above the sea level

5 San Carlo sand monotonic and cyclic characterization

All the soil retrieved from the sub-unit U3 (undisturbed and core samples) was mixed to obtained a material with a grain size distribution 'representative' of the whole unit (a sort of weighted average), which was defined San Carlo Sand, SCS. The grain size curve of SCS is shown in Fig. 8, compared to the curves of the natural sand. SCS has 12.5% of fines and a mean grain size $D_{50} = 0.21$ mm. Its specific gravity and minimum and maximum dry density are: $G_s = 2.672$, $\gamma_{min} = 13.37$ kN/m^3, $\gamma_{max} = 16.95$ kN/m^3, respectively. It is composed by 58.7% quartz, 17.3% feldspar, 17.4% calcite, 3.6% muscovite, 2.2% chlorite and 0.2% kaolinite, as deduced from x-ray diffraction.

The mechanical behaviour of SCS was investigated through a series of monotonic and cyclic Tx tests. The monotonic tests were performed both on undisturbed and reconstituted samples. The cyclic tests were all carried out on reconstituted specimens. The reconstitution was carried out by pluvial deposition in air of the dry sand. All the tested specimens were saturated in the triaxial cell with CO_2 circulation, flushing of deaerated water and adequate back pressure (large enough to avoid cavitation when the soil develops negative pore water pressure). The value of the Skempton parameter B, measured at the end of the saturation, was always higher than 0.98 and the complete saturation was confirmed by compression wave velocities measured after consolidation.

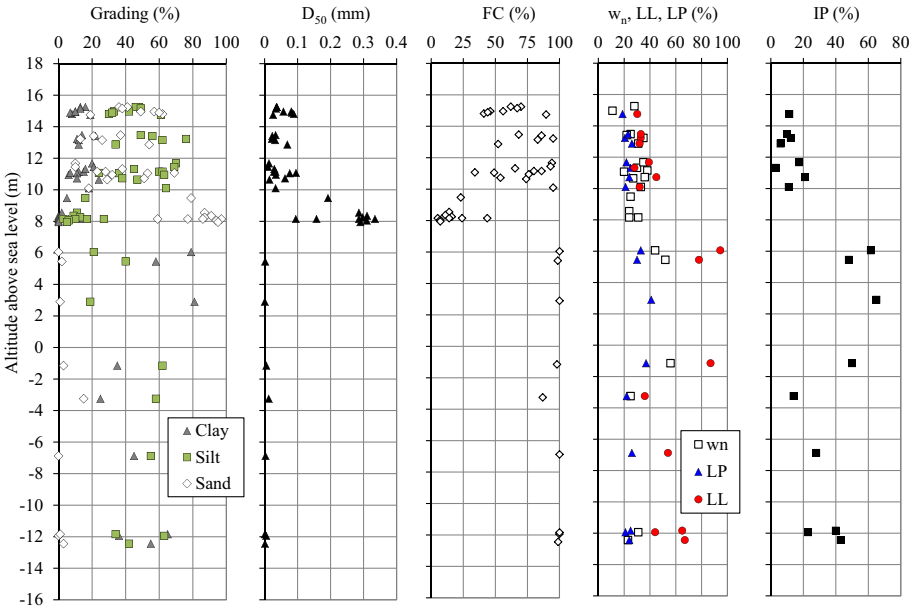

Fig. 7 Results of index tests on undisturbed samples

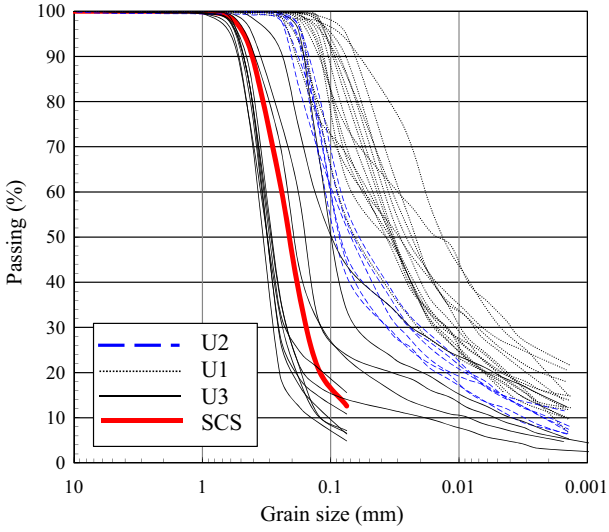

Fig. 8 Grain size curves measured on undisturbed samples and SCS grain size distribution

The monotonic tests consisted of Tx compression on isotropic consolidated specimens. The specimens where normally consolidated using a mean effective stress p'_c ranging from 50 to 600 kPa. Failure was reached applying standard undrained compression stress paths. The results of the tests are shown in Fig. 9, in terms of: void ratio, e, versus mean effective stress, p' (Fig. 9a); stress deviator, q versus p' (Fig. 9b); excess pore pressure, Δu versus axial strains, ε_a (Fig. 9c) and stress ratio, q/p' versus ε_a (Fig. 9d). In Fig. 9a, b the states of the samples at the end of the consolidation are represented by empty triangles.

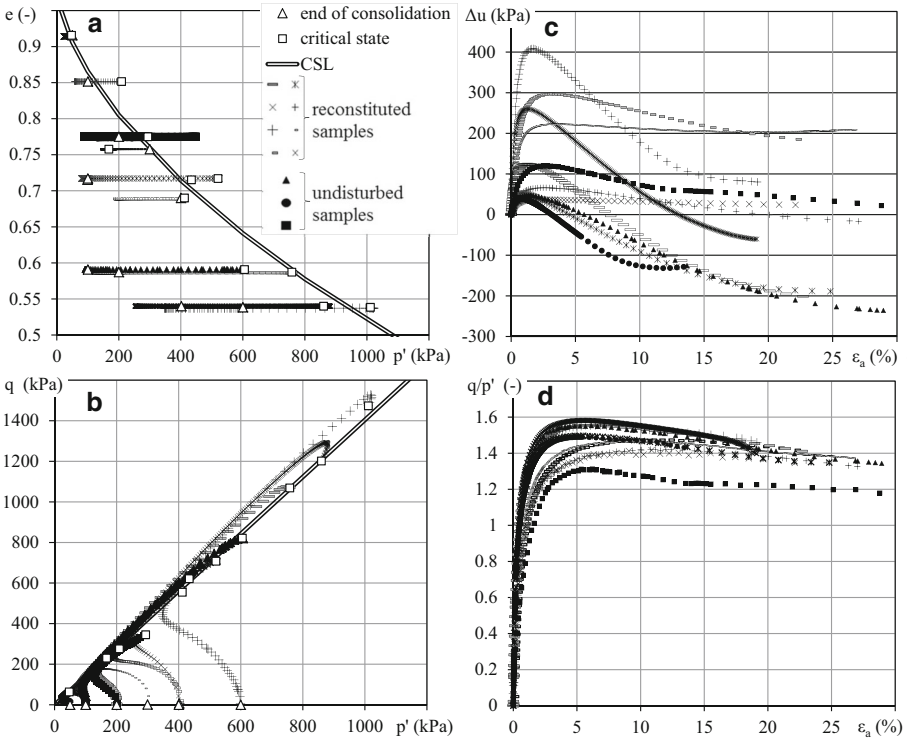

Fig. 9 Monotonic test results: **a** void ratio e versus mean effective stress p′; **b** stress deviator q versus p′; **c** excess pore pressure Δu versus axial strains ε_a and **d** stress ratio q/p′ versus ε_a

As highlighted in the figures, after an initially contractive response (positive pore pressure increment), a marked trend towards dilative response (negative pore pressure increments) was experienced by all specimens. As a consequence of the dilative response, associated with both the development of negative excess pore pressure increments and the increase of the mean effective stress, the undrained stress paths did not exhibit any temporary drop of deviatoric stress and q reached its maximum value at large strains, where the critical state conditions were progressively attained. The critical state conditions were reached by most specimens. In Fig. 9a, b the states of the samples at critical state are represented by empty squares.

The experimental critical state conditions in the q–p′ plane can be interpolated by a linear relationship, which defines the critical state line (CSL), i.e. $q = 1.4p'$ or $M_c = q/p' = 1.4$, where M_c is the strength parameter at critical state in compression loading. The CSL shown in Fig. 9b corresponds to an angle of shearing resistance at critical state $\varphi'_{cs} = 34.7°$.

The critical state data plotted in Fig. 9a, can be fitted by a power function, which, according to Li and Wang (1998), defines the CSL in the e–p′ plane and whose best fit is given by:

$$e_{cs} = 0.99 - 0.12 \cdot (p'/p_a)^{0.59} \quad [-] \tag{1}$$

It's worth noting that the dilative response observed in all tests is explained by the state of the specimens at the end of the consolidation, all lying below the CSL. All the tested specimens, even those characterised by very high void ratio, had negative state parameter ψ at the beginning of the undrained compression, ψ being defined, according to Been and Jefferies (1985), as:

$$\psi = e - e_{cs} \quad [-] \tag{2}$$

where e is the current void ratio and e_{cs} is the void ratio on the CSL at the same p'.

The undrained cyclic Tx tests on SCS were performed on reconstituted samples isotropically normally consolidated at a mean effective stress $p'_c = 100$ kPa. Only two samples were compressed under an isotropic pressure of 150 kPa.

The tested specimens were reconstituted at three values of void ratio: high void ratio ($e_{avg} = 0.78$, which, with reference to Eqs. 1 and 2, corresponds to $\psi_{avg} = -0.073$), medium void ratio ($e_{avg} = 0.73$, $\psi_{avg} = -0.134$) and low void ratio ($e_{avg} = 0.64$, $\psi_{avg} = -0.226$). All the specimens were characterised by negative ψ at the end of consolidation, as represented in Fig. 10, where the initial states of the tested samples are plotted in the e–p' plane. All the samples experienced cyclic mobility, as shown in Fig. 11, where the results of the test MIX1_6 are reported: the axial deformation, ε_a is plotted versus the number of cycles, N in Fig. 11a; the deviatoric stress, q is represented versus ε_a in Fig. 11b; Fig. 11c shows the excess pore pressure, Δu versus N and Fig. 11d reports q versus the mean effective stress, p'. The sample was subjected to a stress deviator $\Delta q = \Delta\sigma_a = \pm 48$ kPa (i.e. to a cyclic stress ratio $CSR^{TX} = \Delta\sigma_a/2p'_c = 0.24$) and reached the failure condition, assumed in this study as the states at which $\varepsilon_a^{DA} = 5\%$, in 5.5 cycles.

At this point the pore pressure ratio, defined as:

$$R_u = \Delta u/p'_c \quad [-] \tag{3}$$

was equal to 0.9.

All the failure conditions of the tested samples are given in Table 4 and represented in Fig. 12, in terms of applied cyclic stress ratio and number of cycles at $\varepsilon_a^{DA} = 5\%$. In the figure, the cyclic stress ratio from triaxial condition (CSR^{TX}) is corrected into cyclic stress ratio for simple shear conditions (CSR^{SS}) according to Ishihara et al. (1977) and Ishihara et al. (1985):

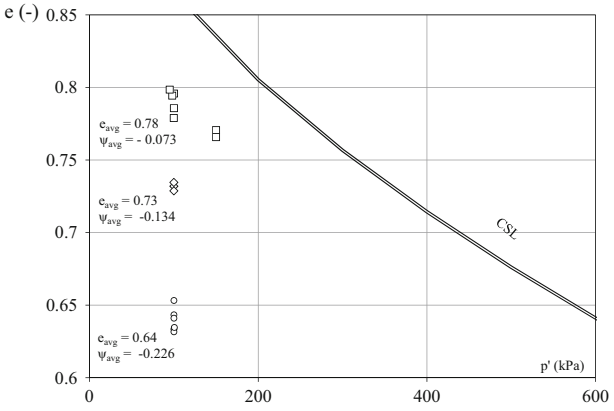

Fig. 10 States after consolidation of specimen subjected to undrained cyclic triaxial tests in the e–p' plane

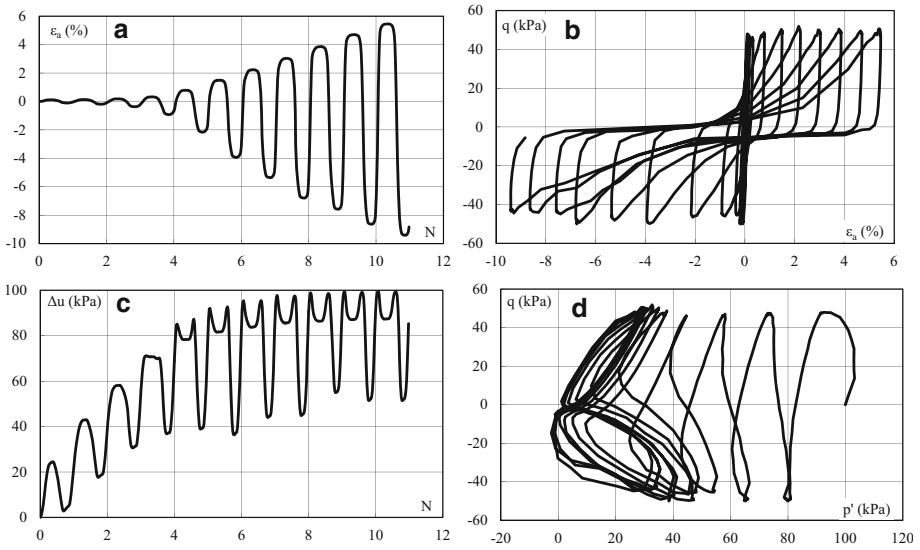

Fig. 11 Results of the cyclic test MIX1_6: **a** axial deformation ε_a versus the number of cycles N; **b** deviatoric stress q versus ε_a; **c** excess pore pressure Δu versus N and **d** q versus the mean effective stress p'

$$CSR^{SS} = CSR^{TX}(1 + 2k_0)/3 \quad [-] \tag{4}$$

where $k_0 = \sigma'_r/\sigma'_a = 0.43$ = stress ratio at rest, computed as a function of φ'_{cs} for normally consolidated samples using the equation of Jaky (1944). Application of Eq. (4) gives $CSR^{SS} = 0.62 \cdot CSR^{TX}$.

The pore pressure ratio R_u values at failure were generally larger than 0.9. Only three specimens developed pore pressure ratios lower than 0.8, as detailed in Table 4.

The data in Fig. 12 show that groups of samples relating to a given ψ_{avg} describe clear relationships between CSR^{SS} and N, whose slope in the semi-log plane is dependent on ψ.

According to Fioravante and Giretti (2016), these relationships were interpreted with a power function of N, which accounts for the dependence of the cyclic resistance on ψ as follows:

$$CSR^{SS} = \frac{a(1-\psi)^b}{N^{c(1-\psi)}} \quad [-] \tag{5}$$

where $a = 0.115$, $b = 3$, $c = 0.145$ = empirical constants determined by fitting experimental data.

In Fig. 12 are reported three curves computed using Eq. 5 for the three groups of ψ_{avg} tested. Equation 5 allows the estimation of the cyclic resistance ration CRR^{SS} for a number of equivalent cycles, e.g. for $N = 4$, which is the number of equivalent cycles associable to an earthquake of moment magnitude $M = 5.8$, according to the Idriss (1999) approach, it results:

$$CSR_4^{SS} = \frac{0.115(1-\psi)^3}{4^{0.145(1-\psi)}} \quad [-] \tag{6}$$

Table 4 Cyclic undrained triaxial tests on isotropic normally consolidate SCS specimens

Test	End of consolidation			Failure				
	e_c –	p'_c kPa	ψ –	$CSR^{TX\ a}$ –	$CSR^{SS\ a}$ –	N^a –	R_u^a –	N_u^b –
R1	0.79	100	−0.076	0.15	0.09	7.5	0.90	9
R2	0.80	100	−0.066	0.22	0.14	2	0.92	3
R3	0.79	98	−0.069	0.13	0.08	11	0.78	13
R4	0.77	150	−0.057	0.10	0.06	97	0.90	–[c]
R5	0.77	150	−0.062	0.12	0.07	40	0.95	–[c]
R6	0.80	95	−0.067	0.16	0.10	25	0.73	30
R7	0.78	100	−0.083	0.13	0.08	84	0.65	90
MIX1_1	0.73	100	−0.130	0.24	0.15	3.7	0.90	4
MIX1_2	0.73	100	−0.133	0.20	0.12	11.5	0.87	13
MIX1_3	0.73	100	−0.127	0.15	0.09	47.5	0.93	48
MIX1_4	0.63	100	−0.228	0.22	0.14	12	0.95	11.5
MIX1_5	0.63	100	−0.230	0.16	0.10	60.5	0.97	59.5
MIX1_6	0.64	100	−0.218	0.24	0.15	5.5	0.90	7
MIX1_7	0.63	100	−0.227	0.26	0.16	11	0.90	–[c]
MIX1_8	0.64	100	−0.221	0.29	0.18	2.6	0.90	3.2
MIX1_9	0.65	100	−0.209	0.25	0.15	3.6	0.92	4

$R_u = \Delta u/p'_c$

[a] Values at $\varepsilon_a^{DA} = 5\%$

[b] Values at $R_u = 0.95$

[c] The condition $R_u = 0.95$ was not reached

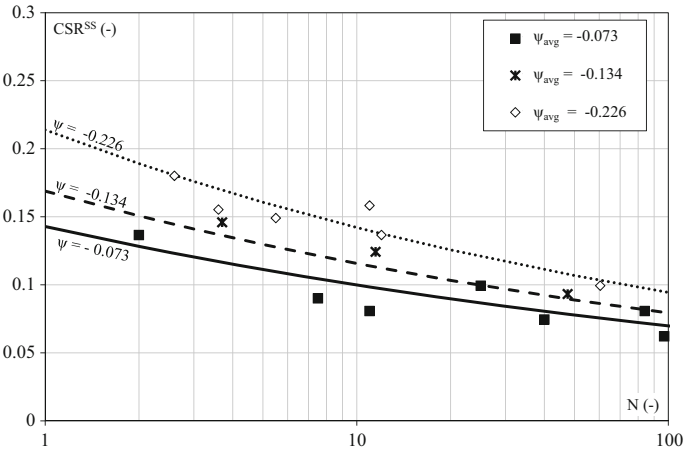

Fig. 12 Cyclic strength of San Carlo Sand in simple shear condition

6 Centrifuge CPTs on San Carlo sand

Four centrifuge CPTs on dry SCS models were carried out at a centrifugal acceleration of 100 g using a miniaturised piezocone and the Istituto Sperimentale Modelli Geotecnici (ISMGEO) seismic geotechnical centrifuge (ISGC), which is a beam centrifuge 6 m in diameter, whose main characteristics are described by Baldi et al. (1988) and Giretti et al. (2012).

The soil models were reconstituted at 1 g by pluvial deposition in air of the dry sand. The pluviation was carried out within a rigid steel cylindrical container (whose internal diameter and height were respectively D = 400 mm and H = 630 mm) by means of a travelling sand spreader. The height of fall of the sand and the dimension of the spreader hole where calibrated in order to obtain the desired soil dry density. The model dimensions where chosen in order to minimise rigid wall boundary effects, according to Bolton et al. (1999). The initial height of the models was 445 mm.

As shown in Fig. 13, where a model scheme is sketched, at the end of the reconstitution, a rigid frame, equipped with the piezocone, two linear displacement transducers (LDT) and a hydraulic actuator, was fixed at the top of the container. The LDTs were used during the tests to monitor the cone displacement and the sand surface settlement.

When loaded in the centrifuge and accelerated to 100 g, the model soil surface settled due to the self-weight of the San Carlo sand, as monitored by LDT. The void ratio at which

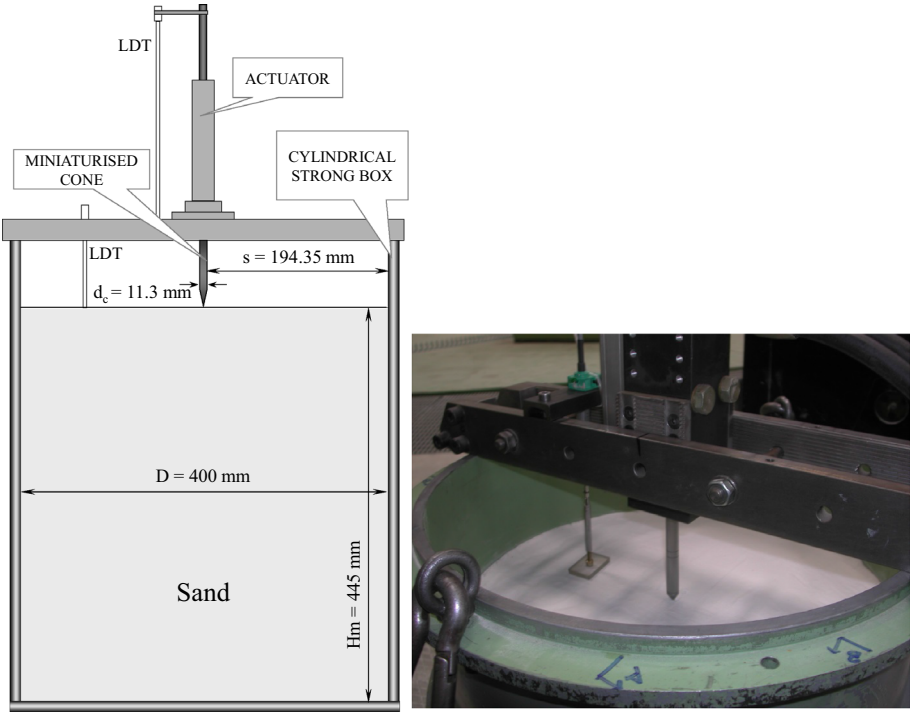

Fig. 13 Model scheme and model picture with a view of the ISMGEO miniaturized piezocone before penetration

the soil was reconstructed, e_0, decreased with depth as computed with the following trial and error procedure. The whole model height was divided into n sub–layers of few millimeters thick. For each ith sub-layer the current values of unit weight and void ratio were computed iteratively as follows:

$$\gamma_{d,i,j} = (G_s\gamma_w)/(1 + e_{i,j}) \quad [FL^{-3}] \tag{7a}$$

$$\sigma'_{v,i,j} = \gamma_{d,i,j} \times t_p + \sigma'_{v,i-1,j} \quad [FL^{-2}] \tag{7b}$$

$$e_{i,j+1} = e_{i,j} - C_c \times \mathrm{Log}(\sigma'_{v,i,j}) \quad [-] \tag{7c}$$

where t_p and $\gamma_{d,i,j}$ are the thickness and dry unit weight of the ith-layer at the jth-iteration and C_c is the average compression index estimated from the total surface settlement of the soil model.

The iteration procedure was concluded after 3 to 5 iterations j, when the convergence error was $|e_{i,j+1} - e_{i,j}| < 10^{-8}$.

The void ratio profiles so calculated were assumed in the computations that follow.

Table 5 reports the average dry unit weight, $\gamma_{dry,0,avg}$ and the average void ratio $e_{0,avg}$ of the models at the end of the reconstruction, the average values of $\gamma_{dry,f,avg}$, $e_{f,avg}$ attained when the centrifuge reached the target speed and the surface settlement was practically completed and finally the value of C_c.

When the inflight surface settlement was completed, the cone penetration test was carried out applying a penetration rate of 2 mm/s. Only one test per model was performed, in the central axis of each sample.

The penetration was interrupted before reaching $20d_c$ of distance from the container bottom to avoid rigid boundary effects (Bolton et al. 1999). In order to take into account the progressive mobilization of the cone resistance from the model free surface (Schmertmann 1978), the measurements registered within a penetration of $10d_c$ from the surface were removed. The measured q_c, not affected by top and bottom boundary effects, is shown in Fig. 14 for each of the models as a function of the mean effective stress p'.

The mean effective stress $p' = \sigma'_v(1 + 2k_0)/3$, of the soil at rest was evaluated from the vertical effective stress σ'_v, which was computed accounting for the acceleration field distortion (i.e.: the centrifugal field increases with the radius from the rotation axis) and

Table 5 Properties of SCS centrifuge models; acceleration a = 100 g

Test	Model reconstruction		Inflight equilibrium				
	$\gamma_{dry,0}$ kN/m^3	e_0 –	s mm	$\gamma_{dry,f,ave}$ kN/m^3	$e_{f,ave}$ –	D_R –	C_c –
SCS1	15.128	0.733	6.17	15.463	0.695	0.64	0.0169
SCS2	14.004	0.872	14.95	14.779	0.774	0.45	0.0441
SCS3	16.155	0.623	1.36	16.233	0.615	0.84	0.0035
SCS4	15.621	0.678	4.56	15.900	0.649	0.75	0.0128

$\gamma_{dry,0}$, e_0 = dry unit weight and void ratio of the reconstituted model

$\gamma_{dry,f,ave}$, $e_{f,ave}$ = average dry unit weight and void ratio of the model after inflight equilibrium

s = soil surface settlement during inflight equilibrium (model scale)

C_c = equivalent compression index

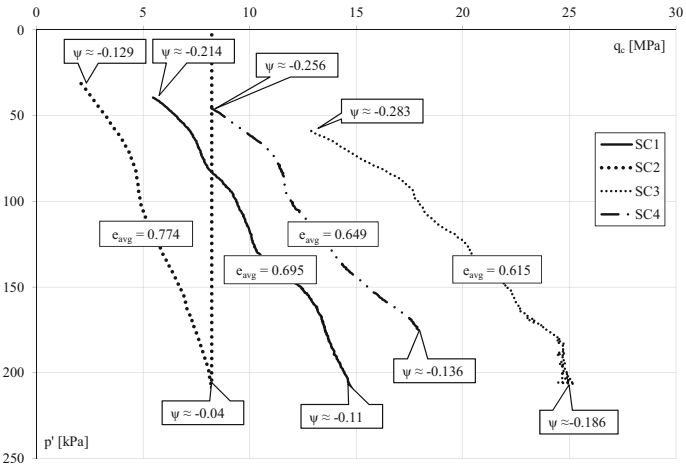

Fig. 14 Centrifuge CPTs in SCS: tip resistance q_c as a function of mean effective stress p'

from the value of $k_0 = \sigma'_h/\sigma'_v = 0.43$ computed according to the Jaky equation (1944) for normally consolidated soils.

The test results show that the soil models were rather homogeneous.

As shown by Carter and Yeung (1985), Carter et al. (1986), Salgado et al. (1997), Jefferies and Been (2006), the zone around the penetrometer is characterized by intense shearing with a significant stress increase around the tip (herein simply referred as $\Delta p'$), with respect to the stress value at rest. $\Delta p'$ is proportional to the volume changes $\Delta\varepsilon$, which in turn can be linked to the value of the state parameter ψ at rest before penetration (Jefferies and Been 2006).

The cone resistance q_c was therefore considered mainly dependent on p' and ψ.

Figure 15 reports the critical state line of SCS; four e–p' traces are also reported: they represent the states of the soil models prior the penetration, from 10 diameter of depth from the model surface to the depth of end of test (first and last relevant points of each test,

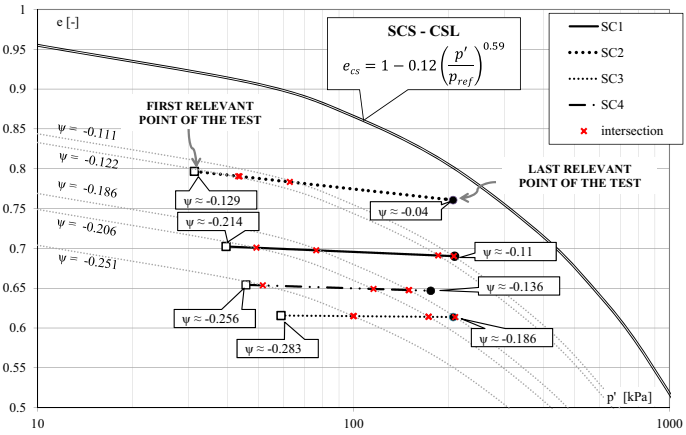

Fig. 15 e–p' relationships of the soil models at rest

respectively). The e–p′ traces are not horizontal lines since they account for the reduction of the void ratio with depth after the achievement the centrifuge target speed. From the soil surface to the maximum depth reached the cone pass through sand with increasing p′ and ψ.

To separate the contributions of p′ and ψ, the following procedure was followed:

1. Effect of p′: each e–p′ profile of the soil models prior to penetration was intersected with constant ψ curves (iso-ψ). The q_c values, measured at depths relating to the intersection, were picked out, normalized by the reference atmospheric pressure (p_a = 101 kPa) and plotted in Fig. 16. The curves in Fig. 16 are constant-ψ–q_c profiles, whose better interpolation are linear functions (in agreement with the observations of Been et al. 1986):

$$q_c/p' = \text{constant} = q_c^* \quad [-] \tag{8}$$

2. Effect of ψ: the q_c^* values obtained from CPTs on SCS models, were plotted versus ψ, as reported in Fig. 17. The $q_c^* - \psi$ trend was interpreted with the equation (adapted from Been et al. 1986):

$$q_c^* = k \cdot e^{-m\psi} \quad [-] \tag{9}$$

where m = 7.42 and k = 27.44 are dimensionless fitting parameter.
The data fitting curve is also plotted in Fig. 17.

7 CRR of SCS from CPT: comparison with an empirical method

To evaluate CRR directly from q_c, the state parameter ψ was assumed to be an independent variable which governs both the cyclic stress resistance and the normalized cone resistance of the tested soil.

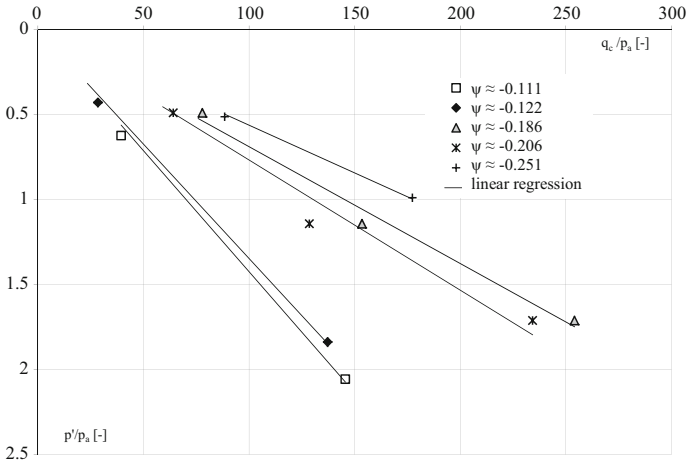

Fig. 16 Cone resistance at constant values of the state parameter ψ

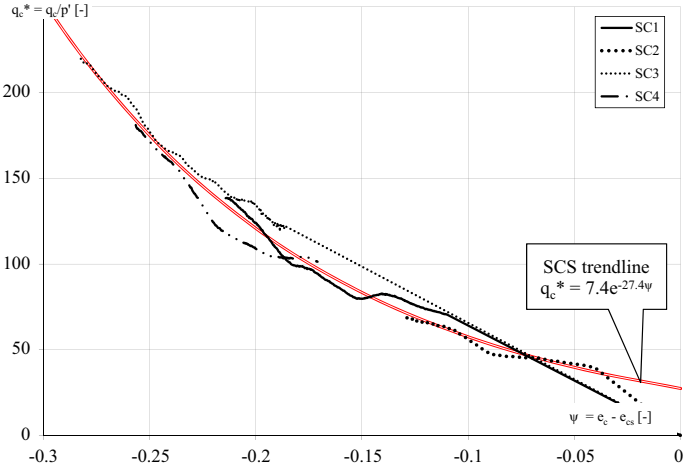

Fig. 17 Centrifuge CPTs in SCS: normalized tip resistance q_c^* as a function of the state parameter ψ

Equations 5 and 9 were combined into Eq. 10 to obtain a direct correlation between q_c^* and the cyclic resistance ratio at N cycles for simple shear condition, CRR_N^{SS}:

$$CSR_N^{SS} = \frac{a\left[1 + \frac{1}{m}\ln\left(\frac{q_c^*}{k}\right)\right]^b}{N^{c\left[1+\frac{1}{m}\ln\left(\frac{q_c^*}{k}\right)\right]}} \quad [-] \tag{10}$$

For N = 4 cycles (corresponding to M = 5.8, Idriss 1999), Eq. 10 can be re-written as:

$$CRR_4^{SS} = \frac{a\left[1 + \frac{1}{m}\ln\left(\frac{q_c^*}{k}\right)\right]^b}{4^{c\left[1+\frac{1}{m}\ln\left(\frac{q_c^*}{k}\right)\right]}} \quad [-] \tag{11}$$

where a, b, c, m and k are the fitting parameters of Eqs. 5 and 9.

The applicability of Eq. 11, to assess the in situ liquefaction susceptibility at the reference site of San Carlo, was tested.

Equation 11 was used to compute a CRR_4^{SS} profile from in situ CPTs for the sand belonging to the sub-unit U3, which was affected by liquefaction during the May 20 earthquake. The CPTUs carried out along the Reno paleochannel (shown in Fig. 6) were selected and the q_c measured between 6.5 and 12 m above the see level were considered as representative of the in situ cone resistance of SCS. From the five q_c profiles the average profile was computed, taking into account the slightly different altitude of the ground level at each test site. The vertical, horizontal and mean stresses were computed assuming a water Table 1 m deep from the ground level and the stress ratio at rest as a function of the angle of shearing resistance of SCS was computed, according to the Jaky equation (1944) for normally consolidated sand. The $q_{c,avg}$ profile was normalized as per Eq. 8 and from the q_{avg}^* values an average CRR profile was computed through Eq. 10 (CRR_{TS}), assuming N = 4. The computed CRR profile is represented in Fig. 18.

In the same figure, the CRR profile, evaluated via a widely used CPT-based simplified approach is plotted. Among others (Seed et al. 1985; Robertson and Wride 1998; Juang et al. 2002, 2006; Cetin et al. 2004; Moss 2003; Moss et al. 2006) the method proposed by

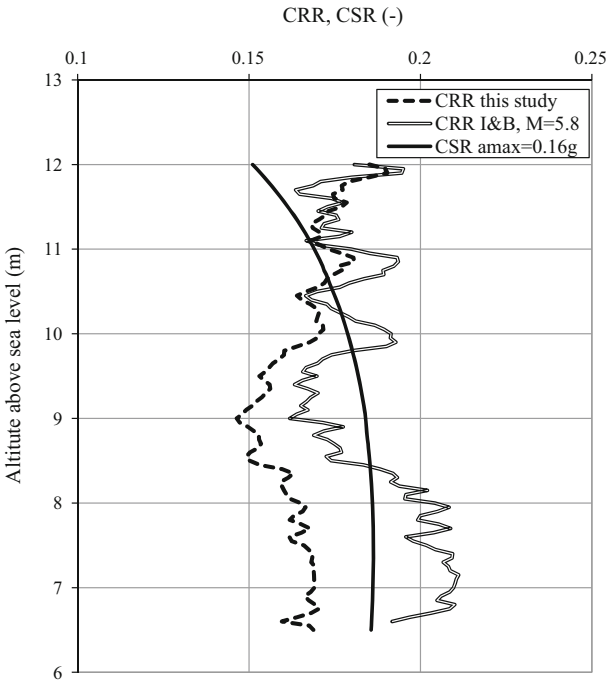

Fig. 18 CRR profiles computed according to Idriss and Boulanger (2008) and the correlation proposed in this study; CSR profile

Idriss and Boulanger (2008) was chosen for the comparison and a $CRR_{I\&B}$ profile was computed as a function of the $q_{c,avg}$ values.

In the computation for CRR, the cyclic resistance, estimated for an earthquake of a conventional magnitude of M = 7.5, was adjusted to a magnitude M = 5.8 through a magnitude scaling factor evaluated according to Idriss (1999):

$$CRR_{I\&B,M=5.8} = CRR_{I\&B,M=7.5} \cdot MSF \quad [-] \tag{12}$$

$$MSF = 6.9\, e^{(-M/4)} - 0.058 \leq 1.8 \quad [-] \tag{13}$$

According to the Idriss and Boulanger (2008) method, $CRR_{I\&B}$ is computed as a function of a normalized cone resistance q_{c1N} corrected into q_{c1Ncs} to take into account the effect of the fine content FC on the cyclic resistance.

The two CRR profiles are compared in Fig. 18 with the cyclic earthquake-induced stresses CSR, which, according to Seed and Idriss (1971), was evaluated as follows:

$$CSR(z) = 0.65 \cdot \left(\sigma_v/\sigma'_v\right) \cdot (a_{max}/g) \cdot r_d(z) \quad [-] \tag{14}$$

where $a_{max} = 0.16$ g = maximum ground surface acceleration estimated for the site of San Carlo for the May 20 earthquake; and r_d = shear stress reduction coefficient, computed as suggested by Idriss (1999).

Figure 18 shows that in the depth interval between 12 and 10.5 m above sea level both the Idriss and Boulanger method and the one presented in this paper forecast a cyclic resistance larger than the earthquake induced cyclic stress. Below 10.5 m down to 6.5 m, according to the Idriss and Boulanger method, only the interval between 9.75 and 8.5 m above the sea level may experience liquefaction, while the CRR profile from this study is

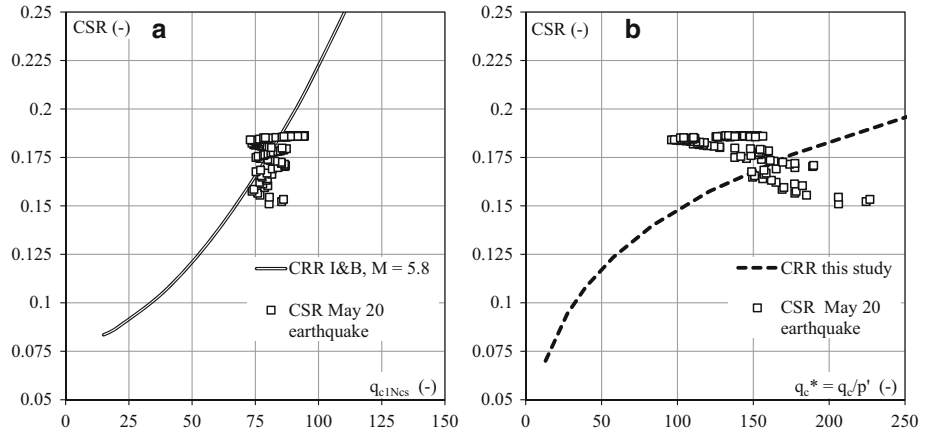

Fig. 19 Curves relating the CRR to the normalized cone resistance according to: **a** Idriss and Boulanger (2008), **b** this study

lower than the CSR curve, indicating a 4 m thick layer of sand susceptible to liquefaction, consistently with the huge amount of sand erupted during the 20 of May earthquake.

The Idriss and Boulanger (2008) method assumes a relationship between CRR and the normalised cone resistance based on a boundary line which separates case histories in which liquefaction was observed from those in which liquefaction was not observed, therefore could have a more general but less site specific validity.

The presented relationship was derived under test conditions as similar as possible to the site conditions:

- all the tests were carried out on the natural sand retrieved at the site of San Carlo;
- the samples were freshly deposited and normally consolidated, similarly to the sand affected by liquefaction at the reference site, which was deposited very recently and didn't experience aging effects, overconsolidation, or cementation;
- the fabric stability that a sand may acquire in situ thanks to the processes of natural deposition in water wasn't reproduced. As a consequence, the experimental cyclic resistance curves should be considered as lower bounds for the tested sand. Same concepts can be applied to the cone resistance from CPTs.

Finally, it would be appropriate to think over on the concavity of the relationships:

CSR, computed according to Eq. 14, is plotted as a function of q_{c1Ncs} in Fig. 19a (Idriss and Boulanger method) and versus q_c^* in Fig. 19b (this study according to Eq. 11). As already found by Fioravante and Giretti (2016) for Ticino and Toyoura sands, the CRR–q_c^* curve calibrated for San Carlo Sand has downward concavity which implies a progressive mobilisation of the cyclic resistance as the normalized cone resistance increases, while the Idriss and Boulanger bounding line could imply an almost infinite cyclic resistance as the normalized cone resistance exceeds a given value.

8 Conclusions

When the cyclic resistance of sandy deposit has to be estimated from cone penetration tests, a soil-dependent calibration in the frame of the critical state soil mechanics is desirable.

The method proposed herein and applied to the case history of the 2012 Emilia earthquake, requires:

- a limited number of triaxial test on reconstituted specimens to establish the critical state line of the sandy soil under examination;
- a limited number of cyclic triaxial or simple shear tests on reconstituted specimens of the soil, in order to define the cyclic resistance of that soil as function of the state parameter.
- a very limited series of cone penetration tests on reconstituted models of the same soil, performed in a large calibration chamber or in a geotechnical centrifuge, in order to define the dependency of the point resistance on the state parameter, assumed as the state indicator on which both CRR and q_c depend.

The state parameter allows the estimation of a site specific correlation between CRR and q_c measured in situ.

The CRR–q_c^* curve calibrated for San Carlo Sand has downward concavity as already found by Fioravante and Giretti (2016) for Ticino and Toyoura sands, which implies a progressive mobilization of the cyclic resistance as the normalized cone resistance increases, consistently with the mechanical behavior of soils measurable in laboratory.

The upward concavity of the traditional simplified approaches bounding lines (which separate the case histories in which liquefaction was or was not observed) implies an almost infinite cyclic resistance as the normalized cone resistance exceeds a given value, consistently with the site detectable effects of liquefaction.

The proposed method follows those developed in the eighties, when the large calibration chambers were developed and a large amount of tests were carried out to establish the correlations between the CPT results and the relative density, the angle of shear resistance or the stiffness of sandy soils (Holden 1971; Reese 1975; Caillemer 1975; Bellotti et al. 1982; Baldi et al. 1982, 1986; Houlsby and Hitchman 1988; Ghionna and Jamiolkowski 1991; Fioravante et al. 1991).

Acknowledgements The Authors gratefully acknowledge the Seismic Surveys of the Emilia-Romagna Regions for having provided the results of in situ tests and the ISMGEO staff (particularly Mr. Sergio Airoldi and Dr. Andrea Saccenti) for having carried out centrifuge and laboratory tests.

References

Baldi G, Bellotti R, Ghionna V, Jamiolkowski M, Pasqualini E (1982) Design parameters for sand from CPT. In: Proceedings of 2nd ESOPT, Amsterdam, the Netherlands

Baldi G, Bellotti R, Ghionna V Jamiolkowski M, Pasqualini E (1986) Interpretation of CPT's and CPTU's 2nd par: drained penetration of sands. In: Proceedings of the 4th international geotechnical seminar. Nanyang Technological Institute, Singapore, pp 143–156

Baldi G, Belloni G, Maggioni W (1988) The ISMES Geotechnical Centrifuge. In: Corté JF (ed) Centrifuge 88, Paris. Balkema, Rotterdam, pp 45–48

Been K, Jefferies MG (1985) A state parameter for sands. Géotechnique 35(2):99–112

Been K, Crooks JHA, Becker DE, Jefferies MG (1986) The cone penetration test in sands: part I, state parameter interpretation. Géotechnique 36(2):239–249

Bellotti R, Bizzi G, Ghionna V (1982) Design, construction and use of a calibration chamber. In: Proceedings of the ESOPT 11, Amsterdam, vol 2, pp 439–446
Bigi G, Bonardi G, Catalano R, Cosentino D, Lentini F, Parotto M, Sartori RSP, Scandone P (1992) Structural model of Italy 1:500,000, CNR-GNDT, Geodinamic Project
Bolton MD, Gui MW, Garnier J, Corte JF, Bagge G, Laue J, Renzi R (1999) Centrifuge cone penetration tests in sand. Geotechnique 49(4):543–552
Caillemer BM (1975) An experimental study in the U.F. static cone calibration chamber, M.Sc. Thesis, Univ. of Florida, Gainesville
Calabrese L, Martelli L, Severi P (2012) Stratigrafia dell'area interessata dai fenomeni di liquefazione durante il terremoto dell'Emilia (Maggio 2012). In: Proceedings of the 31st GNGTS, November 20–22, Potenza, pp 119–125
Carter JP, Yeung SK (1985) Analysis of cylindrical cavity expansion in a strain weakening material. Comput Geotech 1:161–180
Carter JP, Booker JR, Yeung SK (1986) Cavity expansion in cohesive frictional soils. Géotechnique 36(3):349–358
Cetin KO, Seed RB, Kiureghian DA, Tokimastu K, Harder LF, Kayen RE, Moss RES (2004) Standard penetration test-based probabilistic and deterministic assessment of seismic soil liquefaction potential. J Geotech Geoenviron Eng 130(12):1314–1340
Fioravante V, Giretti D (2016) Unidirectional cyclic resistance of Ticino and Toyoura sands from centrifuge cone penetration tests. Acta Geotechnica 11(4):953–968. doi:10.1007/s11440-015-0419-3
Fioravante V, Jamiolkowski M, Tanizawa F, Tatsuoka F (1991) Calibration chamber tests on Toyoura sand. In: Proceeding of the 1st international symposium on calibration chamber testing ISOCCT1 Potsdam New York USA, pp 135–146
Fioravante V, Giretti D, Abate G, Aversa S, Boldini D, Capilleri PP, Cavallaro A, Chamlagain D, Crespellani T, Dezi F, Facciorusso J, Ghinelli A, Grasso S, Lanzo G, Madiai C, Massimino MR, Maugeri M, Pagliaroli A, Rainieri C, Tropeano G, Santucci De Magistris F, Sica S, Silvestri F, Vannucchi G (2013) Earthquake geotechnical engineering aspects of the 2012 Emilia-Romagna earthquake (Italy). In: 7th International conference on case histories in geotechnical engineering, April 29–May 4, 2013, Chicago
Galli P, Melloni F (1993) Nuovo catalogo nazionale dei processi di liquefazione avvenuti in occasione dei terremoti storici in Italia. Il Quaternario 6(2):271–292
Ghionna V, Jamiolkowski MB (1991) A critical appraisal of calibration chamber testing of sands. In: Proceedings of the first international symposium on calibration chamber testing, Potsdam, NY, USA
Giretti D, Fioravante V, Martelli L (2012) Centrifuge tests to evaluate the Po river bank seismic response. In: Proceedings of the 4th international conference on geotechnical and geophysical site characterization (ISC'4), September 15–18, 2012—Porto de Galinhas, Pernambuco, Brazil, pp 1179–1187
Holden JC (1971) Research on performance of soil penetrometers. Country Roads Board of Victoria Internal Report CE-SK-7l-l
Houlsby GT, Hitchman RC (1988) Calibration tests of cone penetrometers in sand. Géotechnique 8(1):39–44
Idriss IM (1999) An update to the Seed-Idriss simplified procedure for evaluating liquefaction potential. Proc, Workshop New Approaches to Liquefaction Analysis, Federal Highway Administration, Washington, DC
Idriss IM, Boulanger RW (2008) Soil liquefaction during earthquakes. Earthquake Engineering Research Institute. MNO-12
Ishihara K, Iwamoto S, Yasuda S, Takatsu H (1977) Liquefaction of anisotropically consolidated sand. In: Proceedings 9th international conference on soil mechanics and foundation engineering, Japanese Society of Soil Mechanics and Foundation Engineering, Tokyo, Japan, vol 2, pp 261–264
Ishihara K, Yamazaki A, Haga K (1985) Liquefaction of K0 consolidated sand under cyclic rotation of principal stress direction with lateral constraint. Soils Found 5(4):63–74
Jaky J (1944) The coefficient of earth pressure at rest. J Soc Hung Archit Eng 78:355–358
Jefferies M, Been K (2006) Soil liquefaction. A critical state approach. Taylor and Francis, London
Juang CH, Jiang T, Andrus RD (2002) Assessing probability based methods for liquefaction potential evaluation. J Geotech Geoenviron Eng 128(7):580–589
Juang CH, Fang SY, Khor EH (2006) First-order reliability method for probabilistic liquefaction triggering analysis using CPT. J Geotech Geoenviron Eng 132(3):337–350
Lavecchia G, de Nardis R, Cirillo D, Brozzetti F, Boncio P (2012) The May–June 2012 Ferrara Arc earthquakes (northern Italy): structural control of the spatial evolution of the seismic sequence and of the surface pattern of coseismic fractures. Ann Geophys 55(4):533–540

Li XS, Wang ZL (1998) Linear representation of steady state line for sand. J Geotech Geoenviron Eng ASCE 124(12):1215–1217

Moss RES (2003) CPT-based probabilistic assessment of seismic soil liquefaction initiation. Ph.D. dissertation, Univ. of California, Berkeley, CA

Moss RES, Seed RB, Kayen RE, Stewart JP, Der Kiureghian A, Cetin KO (2006) CPT-based probabilistic and deterministic assessment of in situ seismic soil liquefaction potential. J Geotech Geoenviron Eng ASCE 132(8):1032–1051

Reese JD (1975) An experimental study on the effects of saturation on the qc and fs values from cone penetration tests in the U.F. Calibration Chamber. M.Sc. Thesis, Univ. of Florida, Gainesville

RER and ENI-Agip (1998) Riserve idriche sotterranee della Regione Emilia-Romagna

Robertson PK, Wride CE (1998) Evaluating cyclic liquefaction potential using the cone penetration test. Can Geotech J 35(3):442–459

Salgado R, Mitchell J, Jamiolkowski M (1997) Cavity expansion and penetration resistance in sand. J Geotech Geoenviron Eng 123(4):344–354

Schmertmann JH (1978) Guidelines for cone penetration test, performance and design, report FHWA-TS-787-209, Federal Highway Administration, Washington, July 1978

Seed HB, Idriss IM (1971) Simplified procedure for evaluating soil liquefaction potential. J Soil Mech Found Div 97(9):1249–1273

Seed HB, Tokimatsu K, Harder LF, Chung RM (1985) The influence of SPT procedures in soil liquefaction resistance evaluations. J Geotech Eng 111(12):1425–1445

Toscani G, Burrato P, Di Bucci D, Seno S, Valensise G (2009) Plio-Quaternary tectonic evolution of the northern Apennines thrust fronts (Bologna-Ferrara section, Italy): seismotectonic implications. B Soc Geol Ital (Italian Journal of Geosciences) 128:605–613. doi:10.3301/IJG.2009.128.2.605